

# Quantum Rotations in Methyl Iodide (CH<sub>3</sub>I)

An experimental investigation using the High-Flux Backscattering Spectrometer and Filter Analyzer Neutron Spectrometer

NIST Center for Neutron Research  
Summer School on Methods and Applications of Neutron Spectroscopy  
June 9-13, 2003

## HFBS Team

Zema Chowdhuri, Craig Brown, and Terry Udovic

### **Abstract**

We will use inelastic neutron scattering to examine the quantum rotational dynamics of methyl iodide (also known as iodomethane, CH<sub>3</sub>I), a textbook example of a symmetric quantum top. The goal of this hands-on measurement is to gain an understanding and appreciation of the backscattering and filter analyzer measurement techniques, get practical experience in obtaining inelastic neutron scattering data, and reduce, analyze and interpret a set of these data.

## Introduction

Methyl iodide is a simple example of a quantum rigid rotor and, as a result, exhibits quantized rotational energy levels. Such rotations take place primarily about the axis aligned with the I and C atoms (see figure 1) and can be measured directly with inelastic neutron scattering. The rotation of the methyl group is detected via scattering of neutrons from the hydrogen atoms. It turns out that hydrogen has an extremely large neutron scattering cross-section, dwarfing the cross-section of carbon by a factor of 15 and iodine by more than 20. An experiment involving scattering from a hydrogenous material like a methyl group yields many scattering events in a short period of time, thus making it ideal to study here.

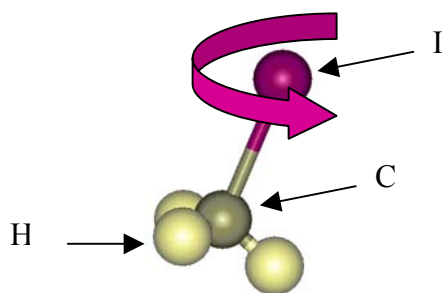
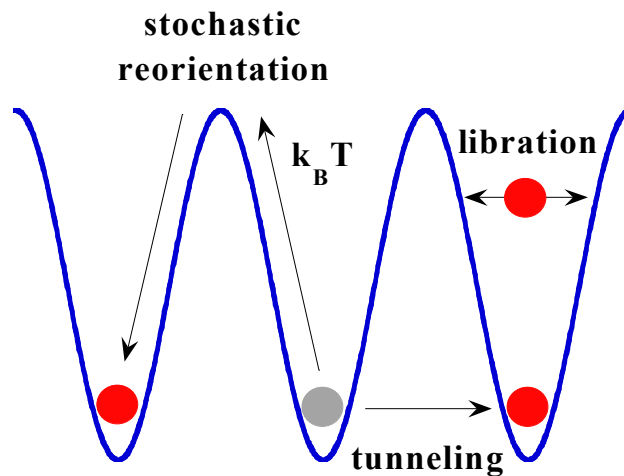


**Figure 1** Schematic of the CH<sub>3</sub>I molecule.

In the solid phase, the CH<sub>3</sub>I molecule is not a free rotor but rather behaves as a single particle confined in a potential well. The existence and characteristics of the potential well are a consequence of the molecule's local environment, and the motion of the molecule is a direct consequence of this confining potential. Since inelastic neutron scattering probes the motion of the molecules (dominated by the H atoms in the molecules), then we should be able to extract information about the confining potential



from the neutron scattering data.

**Figure 2** Schematic illustration of the single-particle picture of the the three types of methyl motion.

This interesting molecular system exhibits dynamics on a number of energy scales, and we will be probing the extremely low-energy dynamics ( $\mu\text{eV}$ ) using the cold neutron backscattering spectrometer and the intermediate energy dynamics ( $\text{meV}$ ) using the thermal neutron filter analyzer spectrometer. In a simple picture of solid methyl iodide, the methyl group can have three independent motions shown schematically in figure 2. At low temperature, the wavefunctions of the protons can overlap and the orientation changes by *tunneling* through the potential barrier. The rate of tunneling is proportional to the overlap of the wavefunctions. The methyl group can also undergo torsional oscillation or *libration*. Finally, if there is enough thermal energy in the solid, the methyl group can undergo stochastic reorientation, also known as *jump diffusion*.

In these measurements we will explore the very low-energy dynamics from tunneling to jump diffusion and the higher energy librational transitions. We will see that in raising the temperature the system's dynamics change from purely quantum-mechanical to classical. The *classically forbidden* tunneling motion is akin to you walking unimpeded **through** one of the concrete shields surrounding the neutron guides. From the tunneling measurements, we will be able to estimate the potential barrier height that the methyl group experiences, estimate the radius of the methyl group, and predict the librational transition and compare it to the measured value taken with the Filter Analyzer Spectrometer.

At various points throughout the text we will pose a number of questions delimited from the rest of the text with boxes. These are meant to arouse your curiosity (italicized) as well as ensure that you have learned some of the basic ideas and details of this measurement (not italicized). Some of them can be answered based on information presented in this report while others you will have to find out from us. We begin with the following question:

Q: *Do you expect the transition energies associated with libration to be higher or lower than those associated with rotational tunneling? Explain your response qualitatively.*

## Sample and Sample Environment Details

Methyl iodide is a liquid at room temperature and solidifies at  $-66.5^\circ\text{C}$ . A small amount of the liquid has been placed into an annular aluminum sample can at room temperature. The annular geometry was selected to minimize the amount of corrections necessary in the data reduction. If the sample is too thick, then a significant number of the neutrons may get absorbed. This *self-shielding* depends on the absorption cross-section of the sample as well as the geometry. For an annular geometry where the neutron sees only a thin portion of the sample, the corrections are negligible. Another concern when determining sample design is minimization of *multiple scattering*. In an ideal neutron scattering measurement, we would like for the neutron to scatter once within the sample before reaching the detector. In practice, the neutrons can undergo multiple scattering events within the sample and/or be absorbed by the sample, the number of such events

increasing with the thickness of the sample illuminated by the beam. One often used rule-of-thumb is to design a sample geometry where 90% of the incident neutrons are transmitted in the forward direction. This is a good compromise between signal and the effects of multiple scattering. Such a sample is usually referred to as a *10% scatterer*. Using the known scattering and absorption cross-sections for CH<sub>3</sub>I and the geometry, one can calculate the desired thickness. For methyl iodide in an annular cell the approximate thickness for 90% transmission in the forward direction is around 0.13 mm. The annular cell we are using provides a sample thickness of about 0.125 mm.

Q: How many times does the beam go through the sample before reaching the detectors?

The answer to the question posed above can have important consequences for your experiment. If the beam passes through the sample twice (for instance) and the sample has an appreciable neutron absorption cross-section, then the intensity at the detectors will be lower than if the beam had only passed once through the sample. Additionally, a beam which passes twice through a strongly scattering sample can produce an energy-dependent background. For more details on these points, see Appendix E.

The sample can have been placed on the cold finger of a closed-cycle refrigerator capable of reaching a base temperature of 8 K. The measurements performed here will span 8 K to 50 K.

### **Spectrometer and Data Reduction Details: HFBS**

The HFBS spectrometer is configured in an *inverse scattering geometry*. This means that the energy of the neutron incident on the sample is varied while the final energy of the neutrons reaching the detectors is fixed.

A summary of the basic principle of operation of HFBS is outlined below:

1. A “white” beam of neutrons back-reflects from the doppler monochromator thus selecting out particular neutron energies,  $E_i$ , dependent upon the speed of the monochromator when reflected. While at rest, only neutrons with a wavelength of 6.27 Å back-reflect from the monochromator. This is due to the lattice spacing of the Si hexagons that tile the surface of the monochromator support.
2. The reflected neutrons scatter from the sample.
3. Only neutrons with a particular scattered energy,  $E_f$ , reflect from the analyzer array into the detectors. Identical Si hexagons comprise the analyzer system, thus the backscattered neutrons all have a wavelength of 6.27 Å. The energy transfer imparted on the sample is defined as  $E = E_i - E_f$ .
4. Neutrons scattered from the sample in a particular direction back-reflect from particular analyzers in one of the 16 detectors. This direction is given by the scattering angle,  $2\theta$ .

Q: What is the energy range of the neutrons incident on the sample,  $E_i$ ? What is the fixed final energy of the neutrons reaching the detectors,  $E_f$ ?

Given the scattering angle,  $2\theta$ , and energy transfer,  $E$ , we may calculate the magnitude of the momentum transfer delivered to the sample,  $Q$ . Kinematical arguments lead to the following relationship between  $2\theta$ ,  $E$ ,  $E_i$ , and  $Q$ :

$$\frac{\hbar^2 Q^2}{2m_n} = 2E_i - E - 2\sqrt{E_i(E_i - E)} \cos 2\theta \quad (1)$$

where  $m_n$  is the mass of the neutron and  $\hbar$  is Planck's constant.

The data acquisition system records the number of detector counts as a function of initial neutron velocity,  $v_i$ , where  $v_i$  is related to the instantaneous monochromator velocity,  $v_m$ , and the Bragg velocity of the neutrons with wavelength  $6.27 \text{ \AA}$ ,  $v_B$ , via  $v_i = v_B + v_m$ . The energy transfer to the sample, due to a Doppler shift of the neutron energies, is given by,

$$E = 2E_B \left( \frac{v_m}{v_B} \right) + E_B \left( \frac{v_m}{v_B} \right)^2, \quad (2)$$

where  $E_B$  is the Bragg energy of neutrons with wavelength  $6.27 \text{ \AA}$ , is calculated and written to the raw data file. Note that the motion of the monochromator is time-dependent, allowing the variation of  $E_i$  necessary to an inverse geometry spectrometer. The raw data measured is recorded as  $N(2\theta_j, E_k) = N_{j,k}$ , the number of neutrons detected in detector  $j$  (at scattering angle corresponding to  $2\theta_j$ ) with an energy transfer to sample of  $E_k$ .

The quantity which reflects the dynamics of the scattering system most directly is  $S(Q, E)$ , the dynamic structure function. What we measure,  $N_{j,k}$ , is closely related to the partial differential cross-section,  $\frac{d^2\sigma}{d\Omega dE}$ . This can be written in terms of the various instrument-dependent parameters and the number of counts received in the detectors,

$$\left. \frac{d^2\sigma}{d\Omega dE} \right|_{j,k} = \frac{N_{j,k}}{\eta(E_f)} \frac{A\eta(\text{FC})}{N(\text{FC})} \gamma_j \frac{1}{\rho_N V} \frac{1}{\Delta\Omega_j} \frac{1}{\Delta E}, \quad (3)$$

where

- $\eta(E_f)$ : efficiency of a  $^3\text{He}$  detector at the fixed final energy,  $E_f$ , of the spectrometer
- $A$ : area of incident beam
- $\eta(\text{FC})$ : efficiency of beam monitor
- $N(\text{FC})$ : total number of counts received in the beam monitor

$\gamma_j$ : efficiency correction factor for detector j  
 $\rho_N$ : number density of scatterers in the sample  
 $V$ : volume of sample illuminated by the beam  
 $\Delta E$ : energy channel width  
 $\Delta\Omega_j$ : solid angle subtended by detector

We can obtain the dynamic structure function [1],  $S(Q,E)$ , using the first Born approximation (i.e. a single scattering event dominates the response of the scattering system) via

$$S(Q,E) = \frac{4\pi}{\sigma} \frac{k_i}{k_f} \frac{d^2\sigma}{d\Omega dE}, \quad (4)$$

where

$\sigma$ : scattering cross-section  
 $k_i$ : incident neutron wavevector  
 $k_f$ : final neutron wavevector

Note that for a sample in thermal equilibrium, the *detailed balance condition* is satisfied,

$$S(Q,-E) = e^{-\frac{E}{kT}} S(Q,E), \quad (5)$$

where  $E$  is the sample energy gain [1]. This condition is a technical way of saying that it is more likely that a sample will give energy to the neutron when the sample is at a high temperature as compared to when the sample is at a low temperature.

### **Spectrometer and Data Reduction Details: FANS**

The FANS spectrometer is also configured in an *inverse scattering geometry*. In the particular instrument configuration for this measurement, the neutrons from the reactor are monochromated with a graphite monochromator. The energy selected from the beam is determined by changing the monochromator angle with respect to the incident beam. This monochromatic beam then hits the sample and scatters into a low-bandpass filter comprised both of polycrystalline Be and graphite. The filter analyzer is so-named because it only transmits scattered neutrons with a fixed final energy of less than 1.8 meV. Essentially, neutrons with wavelengths longer than the Bragg cutoff  $2d_{\max}$  (where  $d_{\max}$  is the maximum interplanar spacing) of the filter material are transmitted with no attenuation due to Bragg scattering. Thus the energy transfer to the sample can be determined by subtracting an average final energy of 1.2 meV from the monochromated incident energy.

The utility of the filter analyzer method for our sample is that the quantity measured is approximately proportional to the density of vibrational (or librational) states. As with

many inelastic neutron scattering spectrometers, the quantity measured with FANS is the neutron partial differential cross-section,  $\frac{d^2\sigma}{d\Omega dE}$ . A number of important factors which are particularly relevant to our sample lead to this approximation. These are: a) the molecules in the scattering system are isolated, b) the atoms in the molecules move independently of atoms in other molecules (the "incoherent approximation"), and c) we are in the low temperature limit ( $k_B T \ll \hbar\omega$ ).

### Methyl Iodide Theory

The simplest picture that describes the low temperature dynamics of CH<sub>3</sub>I begins with an approximate model of the potential energy. To lowest order the (3-fold) symmetry of the methyl group constrains the potential to have 3-fold symmetry. This can be encapsulated in the potential function  $V(\phi) = V_3(1 - \cos(3\phi))/2$  where  $\phi$  specifies the orientation of the methyl group with respect to the I-C axis and  $V_3$  is the height of the barrier (shown in fig. 3). In this simple model, an individual molecule can be viewed as having a fixed orientation in one of the potential minima separated by  $2\pi/3$  [2]. This is equivalent to saying that the hydrogen atoms, i.e. protons, are on fixed *labeled* sites. Since the protons are fermions (spin  $1/2$ ), there are three (energetically) equivalent orientations,  $|123\rangle, |231\rangle, |312\rangle$ , known as *pocket states*.

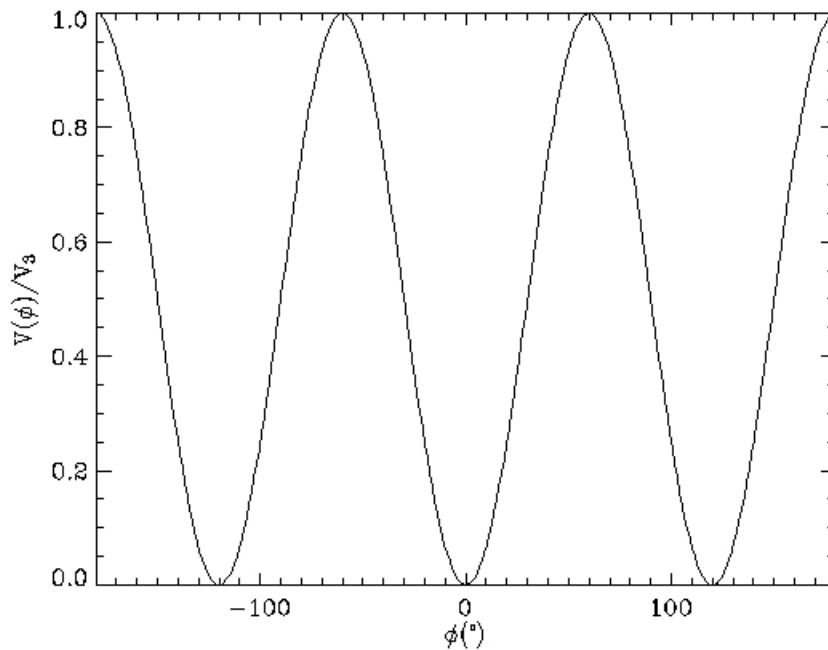


**Figure 3** Simplified three-fold rotational potential for CH<sub>3</sub>I.

Since the molecular motion obeys quantum mechanics the equivalent orientations are not energetically equivalent (i.e. not degenerate). Quantum mechanics requires that the energy levels of the equivalent orientations are split. For very strong potential values, we approach the case discussed in the previous paragraph where the hydrogen atoms are

essentially fixed. In this simple one-dimensional model, there are three types of motion. The first type of motion is a periodic oscillation within the potential well known as a *libration*. The second motion involves the pocket states. Decreasing the potential strength removes the degeneracy of the equivalent pocket states, thus splitting the energy levels so that transitions between the pocket states involves a measurable energy transfer. This phenomenon is known as *tunnel splitting*. In practice the magnitudes of transitions between librational energy levels are on the order of 10 meV whereas those for tunnel splitting can vary between <1 to 100  $\mu\text{eV}$ , at least for splitting of the ground librational state. The final type of motion is *jump diffusion* of the methyl group between the three equivalent orientations. In the single-particle interpretation of this motion, the particle has enough thermal energy to hop over the potential barrier into an adjacent minimum. This is a random motion and manifests itself in the neutron spectrum as a quasielastic peak with a Lorentzian (Cauchy) lineshape.

The usual starting point for an analysis of the quantum mechanics of the methyl groups is the time-independent Schrödinger equation,  $H\Psi = E\Psi$ . In one dimension the Hamiltonian for a rotating methyl group is expressed as

$$H = -\frac{\hbar^2}{2I} \frac{\partial^2}{\partial \phi^2} + V(\phi) \quad (6)$$

where  $I = 5.3 \times 10^{-47} \text{ kg m}^2$  for  $\text{CH}_3$  [3] and  $V(\phi) = V_3(1 - \cos(3\phi))/2$ . Solution of equation (6) can be carried out numerically using the basis functions for free rotors ( $V_3 = 0$ ),

$$\psi_J(\phi) = A_J \exp(iJ\phi). \quad (7)$$

In the case when the potential is zero, the energy levels are given simply by

$$E_J = \frac{\hbar^2 J^2}{2I}, \quad J = 0, \pm 1, \pm 2, \dots \quad (8)$$

Numerical evaluation of Hamiltonian (6) with the basis functions (7) results in the energy levels depicted in figure 4. Those of you who are interested can find the details of the calculation of the energy levels for the rotor in a three-fold potential in appendix A.

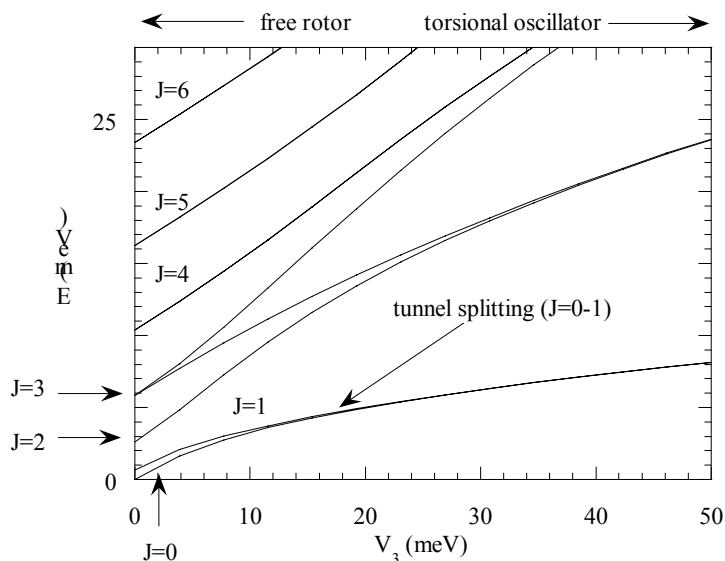


**Figure 4** Energy levels of the rigid rotor as a function of potential strength. The free rotor quantum numbers are listed as well.

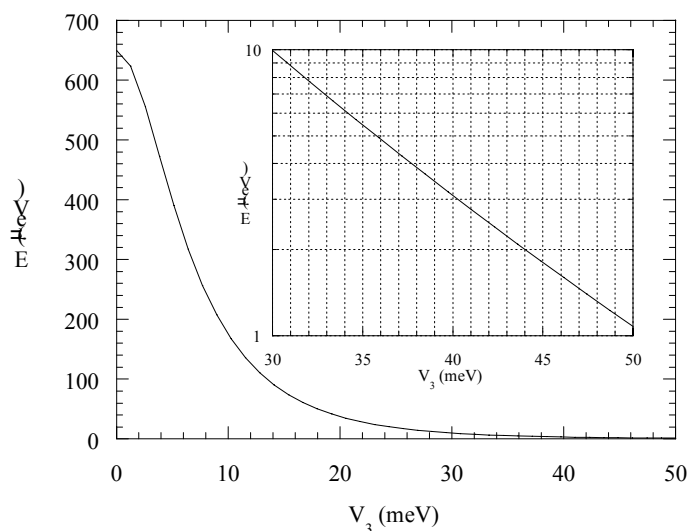


**Figure 5** Energy for the  $J = 0 \rightarrow 1$  transition. Inset is a semilog plot illustrating the approximate exponential dependence of the transition energy with potential.

There are a number of notable features in figure 4. First the energy levels at very small values of  $V_3$  are spaced according to the free-rotor values, given by equation (8). As the strength of the potential increases, some of the branches split apart such as the  $J=3$  and  $J=6$  levels. At high values of  $V_3$ , some of the separate free-rotor energy levels have merged while others are appearing to merge. In particular the  $J=0$  and  $J=1$  levels appear to merge together while the  $J=3$  branch has split and its lower branch seems to merge with the  $J=2$  level. At very high values of  $V_3$  (higher than those displayed in figure 4) many such mergers take place for the higher  $J$  levels. Moreover, small deviations from

the equilibrium orientation are approximately harmonic so that the separation between the librational levels can be expressed approximately as  $3\hbar\sqrt{V_3/2I}$ .

Q: Can you show that the harmonic approximation yields a separation between librational levels of  $3\hbar\sqrt{V_3/2I}$ ? (Hint: Try a small angle approximation to the 3-fold symmetric potential function.)

The ground state tunneling transition is designated as the transition between the  $J=0$  and  $J=1$  states. The energy for such a transition (the difference in energy between the two levels) is displayed in figure 5 for a broad range of potential strengths. The inset illustrates the tunneling transition energy over a smaller potential strength range on a semi-log scale.

### Data Analysis

The reduction and analysis of the data will be discussed by the experimental team but you will be using the software package called DAVE to perform the reduction and analysis. Take a look at some of the low temperature spectra. There are a number of features in the data. The central peak is the elastic scattering from the sample. The two satellite peaks which constitute the inelastic scattering are the tunneling peaks.

The model for tunneling of a methyl group in this type of potential has been worked out [4]. The details are messy and involve calculations of the transitions between the different eigenstates, but the main result is that the intrinsic lineshape is given by

$$S(Q,E) = A_0(Q)\delta(E) + \frac{(1-A_0(Q))}{2} [\delta(E-E_t) + \delta(E+E_t)]$$

$$A_0(Q) = \frac{5 + 4j_0(Qr\sqrt{3})}{9}, \quad (9)$$

where  $r$  is the radius of the methyl group,  $Q$  is the wavevector transfer to the sample,  $E_t$  is the magnitude of the tunneling energy,  $A_0(Q)$  is the elastic incoherent structure factor (EISF), and  $j_0$  is the zero-order spherical Bessel function of the first kind. Note that the lineshape involves three Dirac delta functions in energy, denoted by  $\delta(E)$ . The measured spectrum will be broadened by the instrumental resolution, even at the lowest temperature. See Appendix B for a discussion of the effects of instrumental resolution.

The EISF for a tunneling methyl group is shown in figure 6. In order to extract quantitative information from the data, we must fit equation 9, convolved with the instrumental resolution function, to the data. This fitting can be done within the DAVE software package.

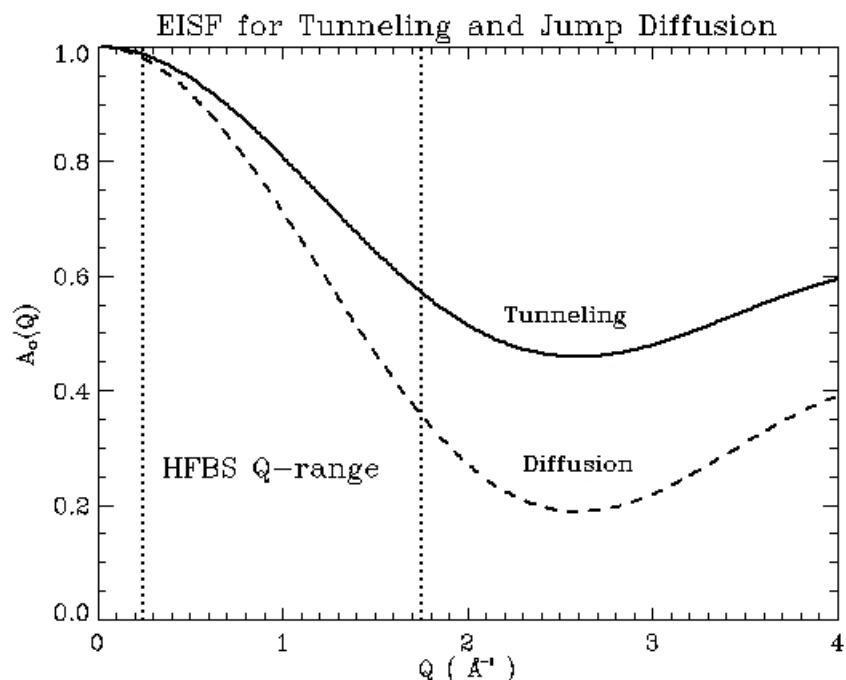


**Figure 6** Elastic incoherent structure factors for a tunneling methyl group (solid line) and a methyl group undergoing three-fold jumps between equivalent orientations (dashed line). Dotted lines indicate the range of the HFBS instrument.

Q: What is your estimate of  $V_3$  based on your low temperature data and the model we have selected?

Q: Based on the barrier height you extracted from the low temperature tunnel spectra, estimate the first librational transition.

Q: What is your estimate of the methyl radius? How does it compare to the accepted proton-proton distance in methyl groups of  $1.78 \text{ \AA}$ ?

The effects of deuteration also have been studied with this system [5]. Hydrogen nuclei are composed of protons but deuterons are composed of a proton and a neutron. Thus we expect the moment of inertia of the rotor to double. The calculation shown in figure 5 has been repeated with such a modification to the moment of inertia and the transition from the  $J=0 \rightarrow 1$  states is displayed over a similar range in figure 7.

Q: If we were to measure  $\text{CD}_3\text{I}$  rather than  $\text{CH}_3\text{I}$ , do you think that we'd be able to observe the tunnel splitting with this spectrometer? Assume that the potential strength does not change from your estimate in the previous question.



**Warning:** the next question is tough!

Q: Explain qualitatively why the tunneling energy decreases when the methyl group is deuterated.

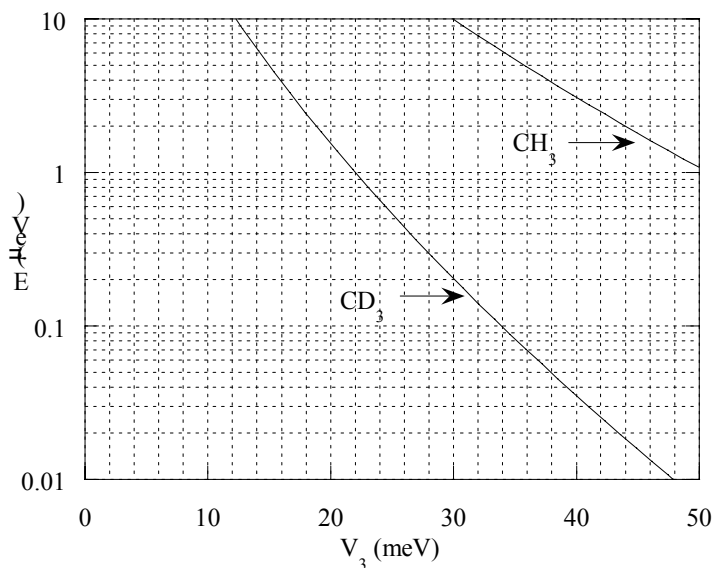


**Figure 7** Potential strength dependence of the one-dimensional rigid rotor  $CD_3I$  and  $CH_3I$  for the  $J = 0 \rightarrow 1$  transition.

As our backscattering measurement proceeds, we will be collecting tunneling spectra at a number of different temperatures to see the temperature dependence of the peak positions.

Q: Does the temperature dependence of the tunneling peaks make sense?

Overnight we will measure a number of temperatures above which you can no longer see any obvious tunneling peaks. The data appears quasi-elastic and this type of data can often be fit with a resolution-broadened elastic peak plus a resolution-broadened Lorentzian lineshape.

$$S(Q, E) = A_0(Q)\delta(E) + (1 - A_0(Q))\frac{\Gamma}{\pi} \frac{1}{E^2 + \Gamma^2}, \quad (11)$$

This model is indicative of a particle undergoing a random reorientation (i.e. hopping) among a small number of equivalent sites. This transition from quantum rotational tunneling to random hopping among three equivalent sites implies a particular EISF

which we can compare to that extracted from our data. For a three-fold jump model on a circle, the EISF is given by [6]

$$A_0(Q) = \frac{1}{3} \left( 1 + 2j_0(Qr\sqrt{3}) \right), \quad (12)$$

which is shown in fig. 6. In addition to having a well-defined EISF, the width of the Lorentzian component of the fit model should be approximately constant with wavevector transfer,  $Q$ .

Q: How well does the model (Eq. 11) describe the data?

The last measurement we perform for this experiment is that of the librational density of states for the CH<sub>3</sub>I.

Q: How does the librational transition as measured on FANS compare with your prediction based on the tunnel spectra?

### References

- [1]. Squires, G.L. *Introduction to the Theory of Thermal Neutron Scattering* ( Cambridge University Press, Cambridge, London, New York, Melbourne, 1978).
- [2]. Prager, M. & Heidemann, A. *Chem.Rev.* **97**, 2933-2966 (1997).
- [3]. Horsewill, A.J. *Spectrochimica Acta* **48A**, 379-403 (1992).
- [4]. Press, W. *Single-Particle Rotations in Molecular Crystals* ( Springer-Verlag, Berlin Heidelberg New York, 1981).
- [5]. Prager, M., Stanislawski, J. & Hausler, W. *J.Chem.Phys* **86**, 2563-2575 (1987).
- [6]. Bée, M., *Quasielastic Neutron Scattering: Principles and Applications in Solid State Chemistry, Biology, and Materials Science* (IOP Publishing, Philadelphia, 1988).

## Appendix A

### Matrix Elements of the 1-D Rigid Rotor in the Three-Fold Potential

The Hamiltonian for the rigid rotor in the three-fold potential is given by equation (6) repeated below

$$H = -\frac{\hbar^2}{2I} \frac{\partial^2}{\partial \phi^2} + V(\phi) \quad (\text{A1})$$

where

$$V(\phi) = \frac{V_3}{2} (1 - \cos 3\phi). \quad (\text{A2})$$

The matrix elements can be calculated using the free-rotor basis eigenfunctions

$$\psi_n(\phi) = \frac{1}{\sqrt{2\pi}} \exp(in\phi), \quad n = 0, \pm 1, \pm 2, \dots \quad (\text{A3})$$

The Hamiltonian (A1) can be decomposed into two parts,  $H_{mn} = H_{mn}^0 + V_{mn}$ , where the elements  $H_{mn}^0$  are related to the zero-potential energy levels as

$$H_{mn}^0 = \frac{n^2 \hbar^2}{2I} \delta_{mn}, \quad (\text{A4})$$

which can be found via the eigenvalue equation for the free rotor Schrödinger equation

$$-\frac{\hbar^2}{2I} \frac{\partial^2}{\partial \phi^2} \psi_n(\phi) = E_n \psi_n(\phi), \quad (\text{A5})$$

with the eigenfunctions given by (A3) and solving for  $E_n$ . The elements of the potential matrix,  $V_{mn}$ , are found by calculating the following integral:

$$V_{mn} = \int_0^{2\pi} d\phi \psi_m^*(\phi) \frac{V_3}{2} (1 - \cos 3\phi) \psi_n(\phi). \quad (\text{A6})$$

Explicit calculation of (A6) and including the zero-potential energy matrix elements (A4) results in the final expression for the matrix elements of the total Hamiltonian:

$$\boxed{H_{mn} = \frac{\hbar^2 n^2}{2I} \delta_{mn} + \frac{V_3}{4} \{2\delta_{n,m} - \delta_{n-m+3,0} - \delta_{n-m-3,0}\}, \quad n, m = 0, \pm 1, \pm 2, \dots} \quad (\text{A7})$$

where  $\delta_{n,k}$  is the kronecker delta,  $\delta_{n,k} = \begin{cases} 1, & n = k \\ 0, & n \neq k \end{cases}$ .

The energy eigenvalues shown in figure 3 were found numerically by generating the matrix,  $H_{mn}$ , for some large number  $N$  (we used 41 which gives sufficient accuracy) for a variety of values of  $V_3$  and calculating the eigenvalues of  $H_{mn}$ .

## Appendix B Instrumental Resolution

In an experiment with an ideal instrument we could measure the sample's scattering response directly. However real neutron spectrometers (and all measurement apparatus in general) have a finite resolution which tends to distort the measured distribution [B1]. The origin of the resolution distortion is due to many instrument-specific factors which lead to an accumulation of (hopefully small!) uncertainties. These uncertainties have the general effect of *blurring* the overall response. The effects of instrumental resolution often can be quantified in the *instrumental resolution function*. Mathematically, the resolution function and the intrinsic scattering function are convolved to yield the measured response. We present here an example of a convolution of two functions and the effects of the resolution width.

In this example we assume that the resolution function,  $R(E)$ , is a normalized gaussian centered at zero,

$$R(E) = \frac{1}{\sqrt{2\pi\sigma^2}} e^{-\frac{1}{2}\left(\frac{E}{\sigma}\right)^2}, \quad [\text{B.1}]$$

and the intrinsic scattering function,  $S(E)$ , is a triangle function centered at zero with a base,  $\Delta$ , one unit wide ( $\Delta=1$ ) and unit height,

$$S(E) = \frac{2}{\Delta} \left[ \left( E + \frac{\Delta}{2} \right) \theta \left( E + \frac{\Delta}{2} \right) - 2E\theta(E) + \left( E - \frac{\Delta}{2} \right) \theta \left( E - \frac{\Delta}{2} \right) \right], \quad [\text{B.2}]$$

where  $\theta(E)$  is the unit step function.

The measured response,  $I(E)$ , is given by the convolution integral,

$$\begin{aligned} I(E) &= R(E) \otimes S(E) \\ &= \int d\tilde{E} R(E - \tilde{E}) S(\tilde{E}), \end{aligned} \quad [\text{B.3}]$$

where  $\otimes$  denotes the convolution operation and the integral is over all values of  $\tilde{E}$ . When the gaussian width parameter  $\sigma$  is small, the gaussian approaches a delta function, and the result of the convolution looks very similar to the original triangle function. Figure B.1 shows this result for a full-width at half maximum (FWHM) of 0.01. When the FWHM is larger, the resulting convolution product looks more distorted and blurred. Figure B.2 shows such a case when the FWHM is 0.5.

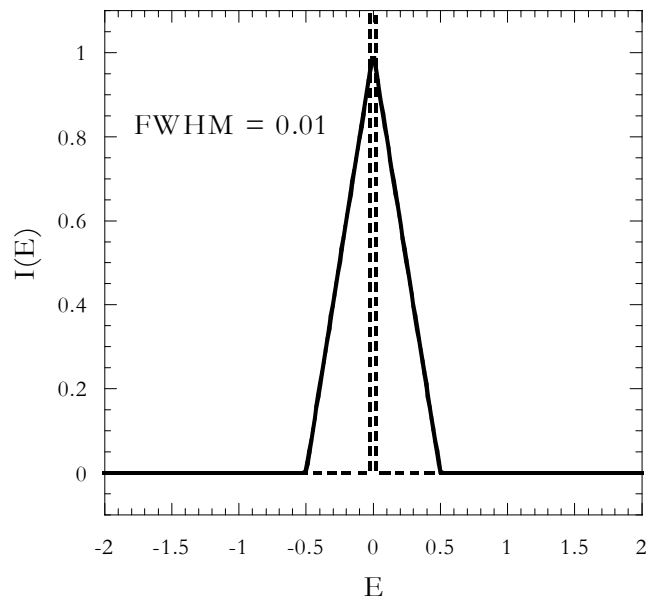


**Figure B.1** Result of the convolution of the triangle function with a gaussian FWHM of 0.01.

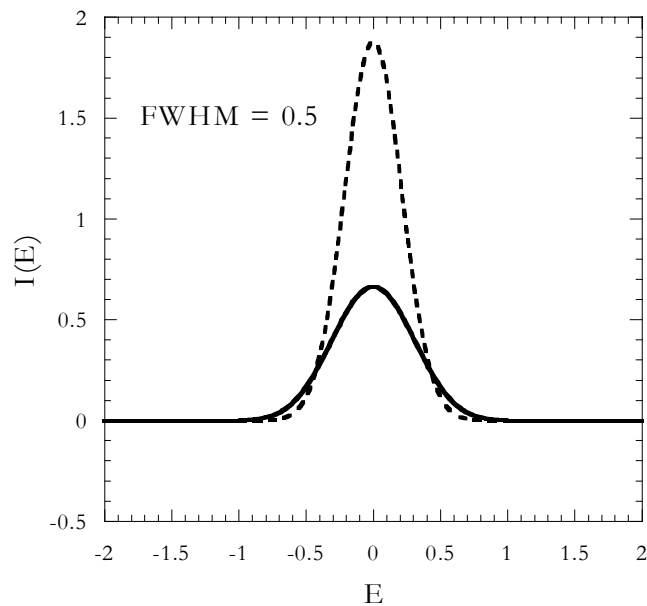


**Figure B.2** Result of the convolution of the triangle function with a gaussian FWHM of 0.5.

Note that as  $R(E)$  becomes more narrow, the convolution product looks more like  $S(E)$ . For a  $\delta$ -function  $R(E)$ , the convolution product is exactly  $S(E)$ . Knowledge of the

instrumental resolution function is essential for detailed lineshape analysis. Often this can be measured using an elastic scatterer.

Q: *How might you use your sample, rather than a vanadium standard (an elastic scatterer) for instance, to measure the instrumental resolution function?*

In many cases, the instrumental resolution can be measured directly and used in the model fitting procedure via the convolution product. If we measure the scattering function from a purely elastic scatterer (ignoring the angular or Q-dependence for now) then the measured quantity is directly proportional to the resolution function. In particular, the elastic scattering function can be represented by a Dirac delta function with area A:  $S_{EL}(E) = A\delta(E)$ . When convolved with the resolution function, we get the measured response:

$$\begin{aligned} I_{\text{meas}}(E) &= A\delta(E) \otimes R(E) \\ &= AR(E) \end{aligned} \quad \text{[B.4]}$$

Note that we must normalize the resolution function so that it has unit area. This is necessary so that we can extract the integrated intensity of the intrinsic lineshape,  $S(E)$ , from the fit to the model. Since the integrated intensity of the convolution product of two functions is equal to the product of the areas of the two functions then, if one of the areas is unity (as in the case of a normalized resolution function), the other must be the total area of the measured intensity.

### References

[B1]. J.T.Grissom and D.R.Koehler, *Am.J.Phys* **35**, 753 (1967).

**Appendix C**  
**Instrument Characteristics for the High Flux Backscattering Spectrometer**  
(<http://www.ncnr.nist.gov/instruments/hfbs>)

Si (111) analyzers covering 20% of  $4\pi$  steradians

Si (111) monochromator 52 cm wide  $\times$  28 cm tall

$\lambda = 6.27 \text{ \AA}$

$E_f = 2.08 \text{ meV}$

$v_n = 630 \text{ m/s}$

16  $^3\text{He}$  detectors covering  $14^\circ < 2\theta < 121^\circ$

Dynamic range:

$-36 \text{ \mu eV} < \Delta E < 36 \text{ \mu eV}$

$0.25 \text{ \AA}^{-1} < Q_{\text{EL}} < 1.75 \text{ \AA}^{-1}$

$\tau \approx 0.1 - 1 \text{ ns}$

Instrumental resolution:

$\delta E < 1 \text{ \mu eV}$  (FWHM)

$\delta Q = 0.1 \text{ \AA}^{-1} - 0.2 \text{ \AA}^{-1}$

Flux at sample:

$\Phi \approx 1.4 \times 10^5 \text{ n/cm}^2/\text{s}$

Beam size at sample:

3 cm  $\times$  3 cm

Signal to noise:

400:1 for vanadium foil (10% scatterer)

Sample environment:

Furnace (300 K – 1700 K)

Closed cycle refrigerator (8 K – 310 K)

Closed cycle refrigerator (30 K – 600 K)

Orange cryostat (1.5 K – 300 K)

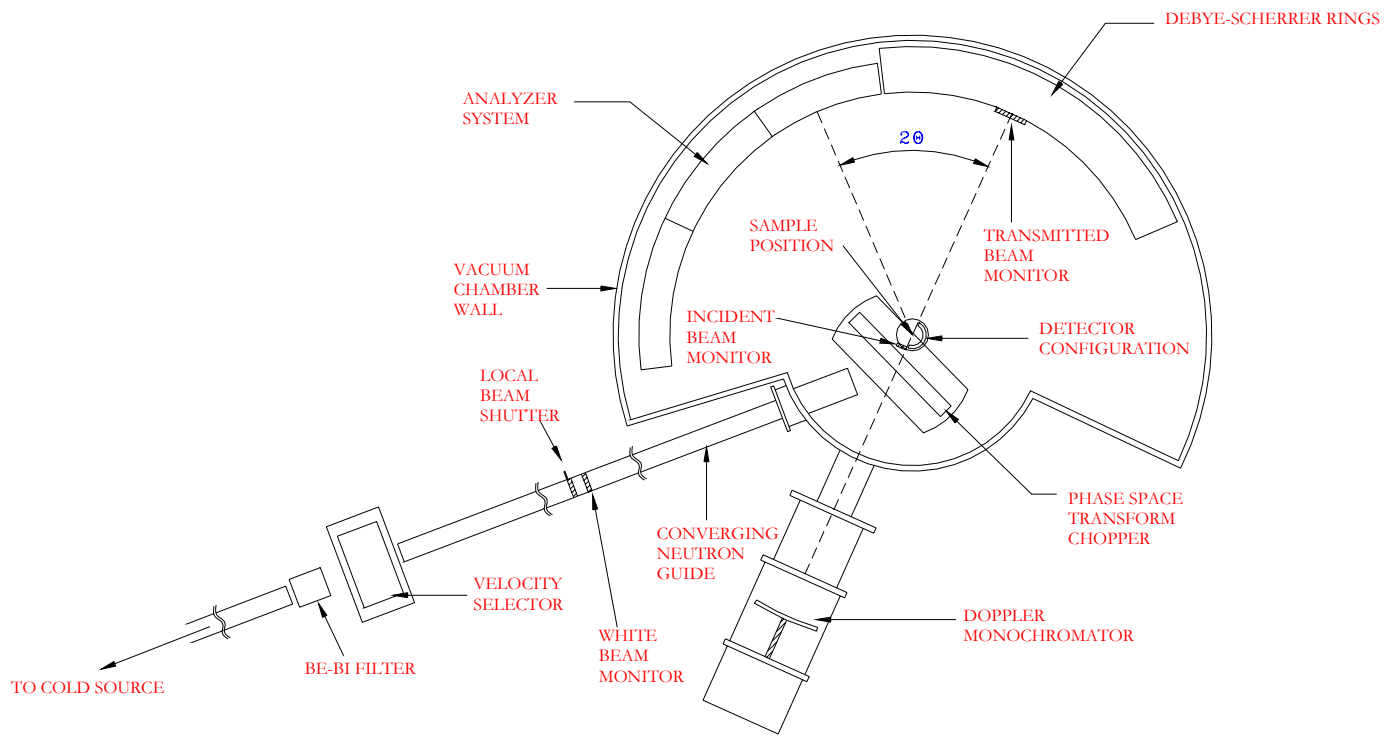


**Figure C.1** Schematic of HFBS

**Appendix D**  
**Instrument Characteristics for the Filter Analyzer Neutron Spectrometer**  
(<http://www.ncnr.nist.gov/instruments/fans>)

- Minimum sample mass 10 mg for a hydrocarbon sample
- Detector coverage: 9% of  $4\pi$  steradians
- $E_f = 1.2$  meV
- 48  $^3\text{He}$  detectors covering  $17.9^\circ < 2\theta < 118^\circ$

Dynamic range:

$$10 \text{ meV} < \Delta E < 250 \text{ meV}$$

Instrumental resolution:

$$\delta E \approx 1.1 \text{ meV at low energy transfer}$$

Flux at sample:

$$\Phi \approx 10^7 \text{ n/cm}^2/\text{s}$$

Beam size at sample:

$$2.5 \text{ cm} \times 6.3 \text{ cm}$$

Sample environment:

Furnace (300 K – 1700 K)

Closed cycle refrigerator (8 K – 310 K)

Closed cycle refrigerator (30 K – 600 K)

Orange cryostat (1.5 K – 300 K)

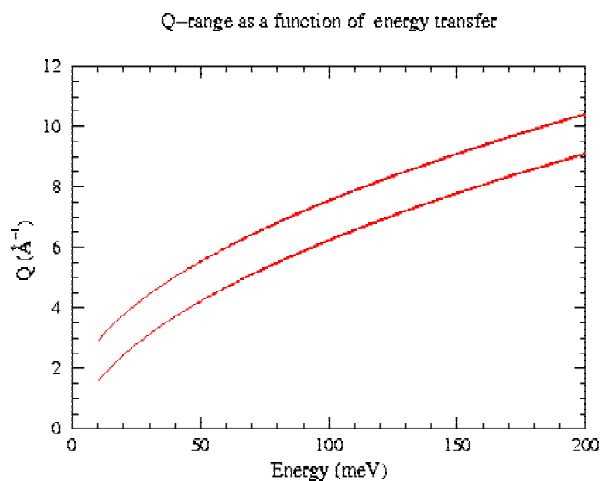


**Figure D.1** Phase space coverage of FANS

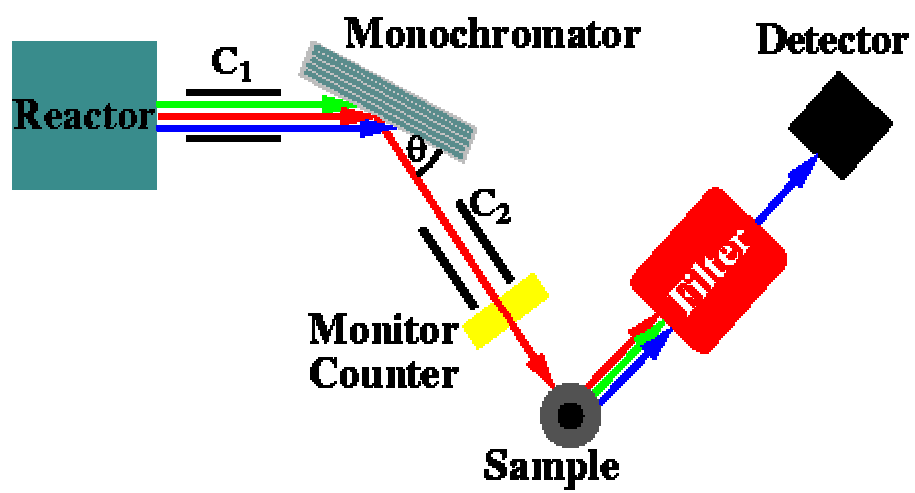


Figure D.2 Schematic illustration of operating principle of FANS

## Appendix E

### Effects of the Sample Geometry on Self Shielding and Multiple Scattering

One must consider a number of issues when determining an appropriate sample geometry. A naïve philosophy in designing a sample geometry is to make the sample as big as possible in order to obtain as many scattering events in the shortest possible time. Unfortunately optimization of the experiment is not as simple as this. Sample design involves a careful consideration of the composition of the sample in terms of its scattering and absorption cross-sections.

In an inverse geometry spectrometer like HFBS where the beam passes through the sample twice one must consider *self-shielding* effects which reduce the intensity received at the detectors via absorption. In general absorption in the sample is proportional to the neutron wavelength. On a backscattering spectrometer using Si(111),  $E_i = 2.08$  meV,  $\lambda = 6.27$  Å, which results in the cross section for absorption being 3.5 times larger than for thermal neutrons with 1.8 Å.

In order to understand the extent to which you have to correct for multiple scattering/self-shielding it is important to know how strong a scatterer/absorber your sample is. The transmission in the forward direction ( $2\theta = 0^\circ$ ) is often calculated and expressed in terms of a percentage of the incident beam that is scattered/absorbed. For instance, a flat plate sample with total scattering cross-section,  $\sigma_{\text{tot}} = \sigma_{\text{inc}} + \sigma_{\text{coh}}$ , and absorption cross-section,  $\sigma_{\text{abs}}$ , will have a scattering and absorption determined by

$$\text{scattering} = 1 - \exp\left(-\frac{\mu_s d}{\sin(\pi - 2\theta)}\right) \quad (\text{flat plate}) \quad (\text{E1})$$

$$\text{absorption} = 1 - \exp\left(-\frac{\mu_{\text{abs}} d}{\sin(\pi - 2\theta)}\right) \quad (\text{flat plate}) \quad (\text{E2})$$

where  $2\theta$  is the angle of orientation of the slab with respect to the incident beam direction,  $d$  is the thickness of the slab sample, and  $\mu$  is the scattering coefficient (inverse scattering length in  $\text{cm}^{-1}$ ) determined by

$$\mu_s = N_A \sigma_{\text{tot}} \rho / A \quad (\text{E3})$$

$$\mu_{\text{abs}} = N_A \sigma_{\text{abs}} \rho / A \quad (\text{E4})$$

where  $N_A$  is Avogadro's number ( $6.022 \times 10^{23}$  mole<sup>-1</sup>),  $\rho$  is the mass density of the sample material (in g/cc), and  $A$  is the molecular weight of the sample in g/mol. On the other hand an annular sample cell has a scattering/absorption in the forward direction determined by

$$\text{scattering} = 1 - \exp(-\pi \mu_s d) \quad (\text{annular cell}) \quad (\text{E5})$$

$$\text{absorption} = 1 - \exp(-\pi\mu_{\text{abs}}d) \quad (\text{annular cell}) \quad (\text{E6})$$

where the inverse scattering/absorption lengths are calculated as described above (eqs. E3 and E4) and  $d$  is the wall thickness of the annular sample. Equations (E5) and (E6) are good approximations for the cases where  $\exp(-\pi\mu d) > 80\%$ .

We illustrate the self-shielding corrections for a vanadium sample ( $\sigma_s(1.8 \text{ \AA}) = 5.10$  barn and  $\sigma_{\text{abs}}(1.8 \text{ \AA}) = 5.08$  barn [E1]) for two different geometries: a flat plate and an annular sample. The intensity in the detectors is very sensitive to the thickness of the sample as well as its geometry. If we assume these two geometries for the same amount of scattering (5%, 10%, and 20% scatterers respectively as calculated via (E1) and (E5)) and assume that the samples are completely illuminated by the incident beam then we obtain the results displayed in figure E.1. The corrected intensity is obtained using  $I_{\text{corr}}(2\theta, E) = I_{\text{obs}}(2\theta, E)/A_{\text{ssc}}$  where  $I_{\text{obs}}(2\theta, E)$  is the observed intensity. It is quite clear that there is a much stronger angle dependence for the correction factor of the slab geometry whereas the corrections are much less for the annular cell. Furthermore, an evaluation of the correction factor is impossible near the orientation angle,  $130^\circ$  in the present example, for the slab geometry. Therefore it is advantageous to use an annular geometry for backscattering. Note that, because the beam goes through the sample twice on HFBS, the sample transmission due to the presence of absorption must be squared.

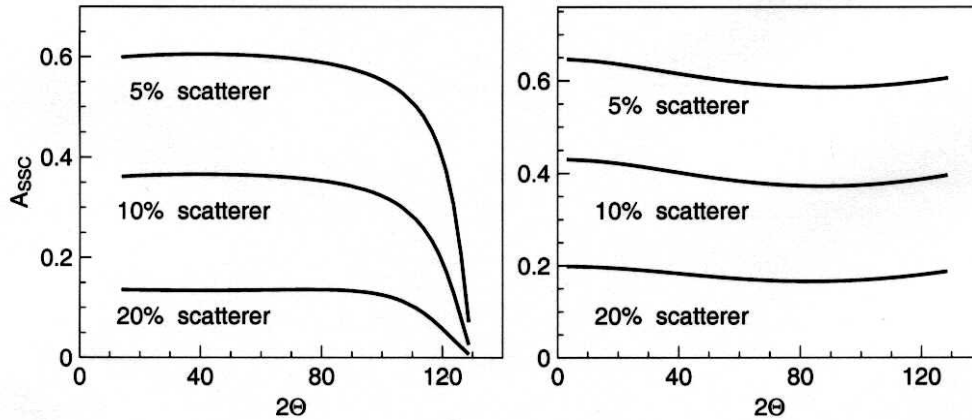


**Figure E.1** Scattering angle dependence of the self-shielding correction factor for (a) flat plate whose normal is oriented  $130^\circ$  with respect to incident beam direction and (b) an annular sample geometry.

When one increases the thickness of the sample for a system with a medium absorption cross-section the intensity will not significantly increase but the effects of multiple scattering will certainly be enhanced. Corrections for multiple scattering are not trivial and, for many systems in which the scattering function is not known a priori, may not be possible at all.

Figure E.2 illustrates the effects that multiple scattering can have on a system, in this case viscous glycerol. This sample was measured on the IN10 backscattering spectrometer at the ILL at a temperature where the structural relaxation (viscous flow) is on the time

scale of the instrument (0.1–1 ns). There is a clear broadening of the lineshape with increasing  $Q$  ( $\text{FWHM} \sim Q^2$ ) due to the dynamics of the system. However at  $Q = 0.19 \text{ \AA}^{-1}$  structural relaxation cannot be resolved because its too slow at this small  $Q$ . The effective broadening in the wings is entirely due to multiple scattering.

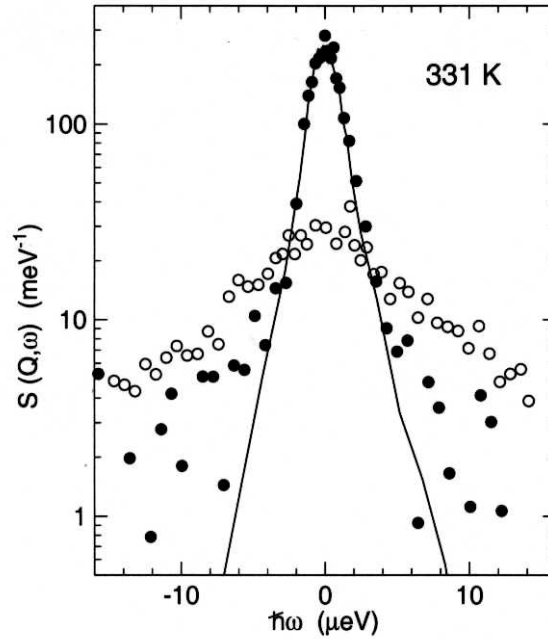


**Figure E.2** Scattering intensity of viscous glycerol taken on the IN10 backscattering spectrometer illustrating the effects of multiple scattering on  $S(Q,E)$ . Solid line represents the instrumental resolution, open symbols are data taken at  $Q=1.4 \text{ \AA}^{-1}$ , and the closed symbols are data taken at  $Q=0.19 \text{ \AA}^{-1}$  [E2].

### References

- [E1]. V.F.Sears, Neutron News **3**, 26 (1992)
- [E2]. J. Wuttke et al., Phys. Rev. E **54**, 5364 (1996)